UNIVERSITÁ DEGLI STUDI DI PADOVA

Dipartimento di Fisica e Astronomia "Galileo Galilei"
Corso di Laurea in Fisica

Tesi di Laurea

Implementation of an Interferometric Measurement System for the Stability of Macroscopic Structures at the Level of the Picometer

Relatore:
Dr. Giacomo Ciani

Laureando:
Michele Martinazzo

Anno Accademico 2017-2018

Contents

Introduction

The experiment described here was born in the context of ALPS experiment (Any Light Particle Search), which aims to detect a particle called axion, a weakly interacting dark matter candidate. The ALPS's experimental setup involves the use of two collinear optical resonators, one for the production of axions by exposing the light to a strong magnetic field (production cavity), and the other one with the purpose of transforming the axions into photons, that are measurable (regeneration cavity). ALPS requires a light-tight very stable central bench, in order to keep the two cavities aligned. However, the LEM (low expansion materials) commonly used in optics physics are not opaque; the ALPS team at the University of Florida designed a composite breadboard in order to solve this issues.

An interferometric measurement system was implemented to study the longitudinal vibrations of the breadboard prototype at the level of precision required from ALPS. An optical cavity (test cavity) was constructed on the breadboard, and placed in a vacuum chamber. A lasers was aligned and mode matched to test cavity, then it was locked to a resonant frequency via Pound Drever Hall technique. The same was done for an ultra-stable reference cavity with another laser in another vacuum tank. The beat note between the two lasers, that contains the information about the test cavity length fluctuations, was sampled and analyzed.

Chapter 1

Background

This chapter introduces the theoretical concepts that underlie the techniques used in this thesis work, such as the gaussian beam, the optical resonators and the techniques used for the stabilization of a laser to an optical cavity.

1.1 Gaussian Beam

In laser physics, laser beams are often studied in the form of gaussian beams, which is the simplest propagation shape taken by a laser electromagnetic field. The name derives from the shape taken by the transverse profile of the laser beam intensity, which is described by a two-dimensional Gaussian curve (equation 1.1.0.6). Gaussian beams are usually considered in situations where the beam divergence is relatively small, and it is possible to apply the paraxial approximation to the wave function. If we have a laser beam that is propagating along the z-axis in free space, we can describe the electromagnetic field according to the Helmholtz equation (for the detailed calculations that lead to the results reported in this section, see [2]) (this equation can be obtained from the wave equation by imposing that the solution is $E(x, y, z, t) = e^{i\omega t} E(x, y, z)$)

$$[\nabla^2 + k^2]E(x, y, z) = 0 \qquad (1.1.0.1)$$

It is possible to write the field $E(x, y, z)$ in the following form:

$$E(x, y, z) = u(x, y, z)e^{-ikz} \qquad (1.1.0.2)$$

Where it was made explicit the oscillatory propagation term along the z-axis e^{-ikz}. The term that we are interested in studying is $u(x, y, z)$, which is the complex scalar wave amplitude and describes the transverse profile of the laser field. Substituting equation 1.1.0.2 inside equation 1.1.0.1 we get:

$$\frac{\partial^2 u}{\partial x^2} + \frac{\partial^2 u}{\partial y^2} + \frac{\partial^2 u}{\partial z^2} - 2ik\frac{\partial u}{\partial z} = 0 \qquad (1.1.0.3)$$

Since in the paraxial approximation the beam intensity falls off quickly as one moves away from the optical axis, the dependence on z of $u(x, y, z)$ is slow compared to that on x or y and it is possible to neglect the second partial derivate in z, obtaining:

$$\frac{\partial^2 u}{\partial x^2} + \frac{\partial^2 u}{\partial y^2} - 2ik\frac{\partial u}{\partial z} = 0 \qquad (1.1.0.4)$$

This approximation is called the paraxial approximation, and the resulting equation takes the name of paraxial wave equation. It is possible to find an analytical form for $u(x, y, z)$:

$$u(x, y, z) = \frac{1}{R(z - z_0)}exp\left[-ik\frac{(x)^2 + (y)^2}{2R(z - z_0)}\right] \qquad (1.1.0.5)$$

Where $R(z - z_0)$ represents the radius of curvature of the spherical wavefront, and the point $(0, 0, z_0)$ is called waist; it is the point where the laser beam has the minimum size. This equation describes the lowest-order solution for the transverse profile of a laser beam in the paraxial approximation [2]. The equation that describes the transverse profile of the optical intensity $I(r, z)$ of the gaussian beam takes the form:

$$I(r, z) = \frac{P}{\pi w\left(z\right)^2/2}exp\left(\frac{-2r^2}{w\left(z\right)^2}\right) \qquad (1.1.0.6)$$

Where $w(z)$ is the beam radius (physically it is distance from the beam axis to where the intensity drops to $\frac{1}{e^2}$ of the maximum value) and P is the power carried by the beam. We can see in this figure above (figure 1.1) the shape of a simulated gaussian beam at an instant of time.
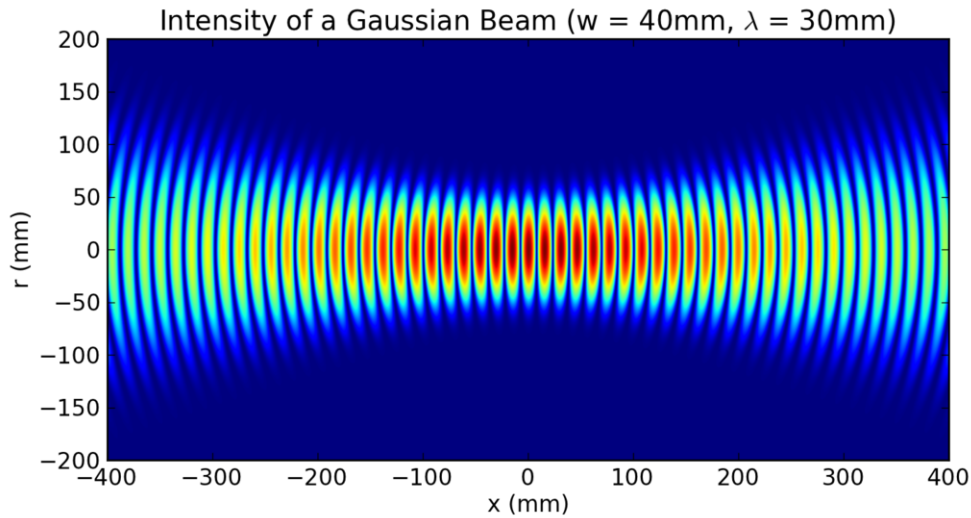
Figure 1.1: Gaussian beam. The curves represent the spherical wavefronts of the beam. Picture credits: $http://en.wikipedia.org/wiki/Gaussian_beam$

For a given wavelength λ of the laser radiation, it is possible to fully characterize a gaussian beam knowing direction of propagation of the beam, waist position and waist spot size. The waist w_0 of the beam is the point where the beam width w(z) is the smallest. From these it is possible to derive all the quantities that describe the gaussian beam.

The Rayleigh range is the distance along the propagation direction of a beam from the waist to the place where the beam radius is $\sqrt{2}$ times the the radius in the waist. It can be expressed as:

$$z_R = \frac{\pi w_0^2}{\lambda} \tag{1.1.0.7}$$

The Rayleigh range can be thought of as the distance within which the gaussian beam propagates without diverging significantly.
The size of the laser beam $w(z)$ along the z-axis is described by the formula:

$$w(z) = w_0 \sqrt{1 + \left(\frac{z}{z_R}\right)^2} \tag{1.1.0.8}$$

Where z is the distance along the optical axis from the waist.
As show in figure 1.1, the curvature of the wavefronts is not constant, but evolves along the z direction according to the formula:

$$R(z) = z + \frac{z_R^2}{z} \tag{1.1.0.9}$$

Note that the wavefront is flat (R=infinite) at $z = z_0$ and when z tends to infinity.

If we observe the field at a sufficiently large distance from the waist, we see from 1.1.0.8 that $w(z)$ increases approximately linearly with distance, and we can define a divergence angle as:

$$\theta = \frac{\lambda}{\pi \omega_0} \qquad (1.1.0.10)$$

that means that the smaller the beam waist size w_0 the faster it will diverge. Figure 1.2 summarizes the fundamental parameter of a gaussian beam.
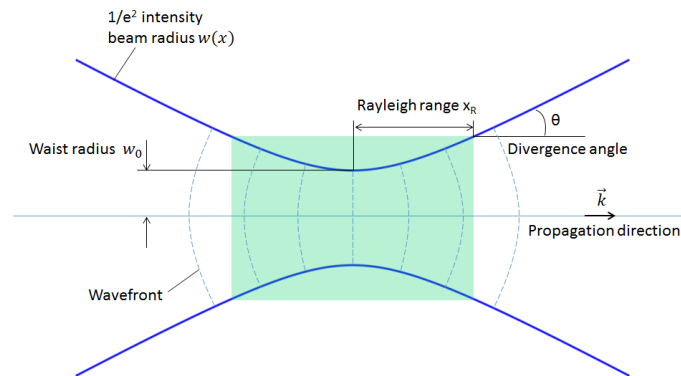

Figure 1.2: Important parameters in a gaussian beam. Picture credits:*https : //www.comsol.com/blogs/understanding − the − paraxial − gaussian − beam − formula/*

1.2 Optical Resonators

An optical resonator, also called optical cavity, is an arrangement of mirrors or optical components that allows a beam to circulate in a close path. It is possible to distinguish two kind of optical resonators [5]:

- Linear resonators; they are made in such a way that the light bounces back and forth between two ends mirrors. The simplest kind of optical resonators, the plane-parallel or Fabry Pérot cavity, belongs to this category.

- Ring resonators; in a ring cavity the laser beam propagates only in one direction, remaining a traveling wave.

The systems that we are interested to study are the stable linear resonators in a homogeneous medium. To understand the property of resonators, it is important to understand the physical mechanism of the resonance.

To obtain resonance it is necessary that the field make constructive interference with itself after a round-trip into the cavity; Generally an electro-magnetic wave, when propagated in space, does not retain its transverse intensity profile. However, there are field distributions that propagate in a self-consistent way; these are called modes. The simplest of these modes is the gaussian mode, which is propagated by maintaining a gaussian transverse profile. There are, however, higher order modes, which are a solution to equation 1.1.0.4 and which represent more complicated transverse distributions. These modes also constitute a series of orthonormal bases, through which one can describe a generic laser beam.

In a stable resonator we can think the light confined inside can be described as an overlap of this spatial cavity modes, which must reproduce their exact transverse amplitude profile after one round trip in the cavity. Moreover the total phase change after one trip must be an integer multiple of 2π.

The most common transverse modes (TEM_{nm}) used to describe the beam inside an optical resonator are the Hermite–Gaussian modes (HG_{nm}) and the Laguerre-Gaussian modes (LG_{nm}), which differ for the symmetry of the transverse intensity profile; the first is characterized by a rectangular symmetry, the second by a cylindrical symmetry. A generic paraxial beam can be described as a transverse modes expansion:

$$E(x, y, z) = \sum_n \sum_m c_{mn} u_n(x, z) u_m(y, z) e^{-ikz} \qquad (1.2.0.1)$$

Where $u_n(x, z)$ are the modes solutions of the equation 1.1.0.4, and c_{mn} are complex coefficients. Depending on the selected coordinates, cylindrical or cartesian, $u_n(x, z)$ will be proportional to Laguerre or Hermite polynomials respectively [2]. n and m represent the number of nodes of the field, which are located along the x and y axis for the Hermite polynomials and along the radius and circumference for those of Laguerre. In Figure 1.3 and 1.4 are shown the lower order transverse modes for the Hermite-Gauss and Laguerre-Gauss bases.
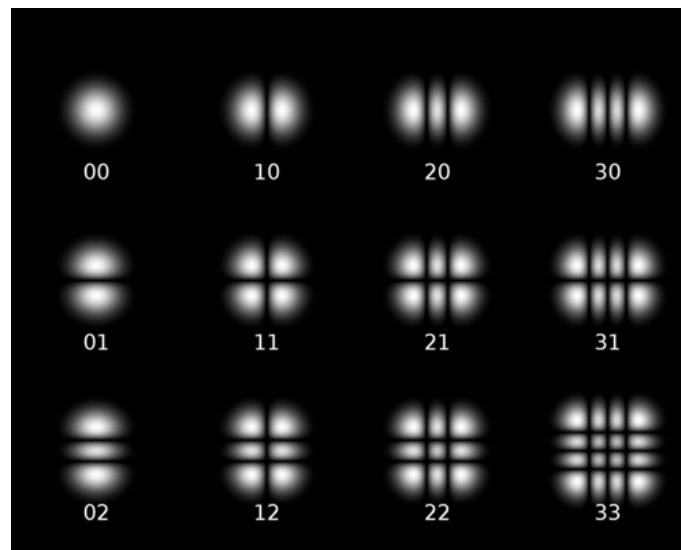
Figure 1.3: Intensity profile of some of the lowest order Hermite-Gaussian Modes. Note that the phase, not represented in this image, varies across the beam profile. Picture credits:*https* : *//en.wikipedia.org/wiki/Transverse mode*
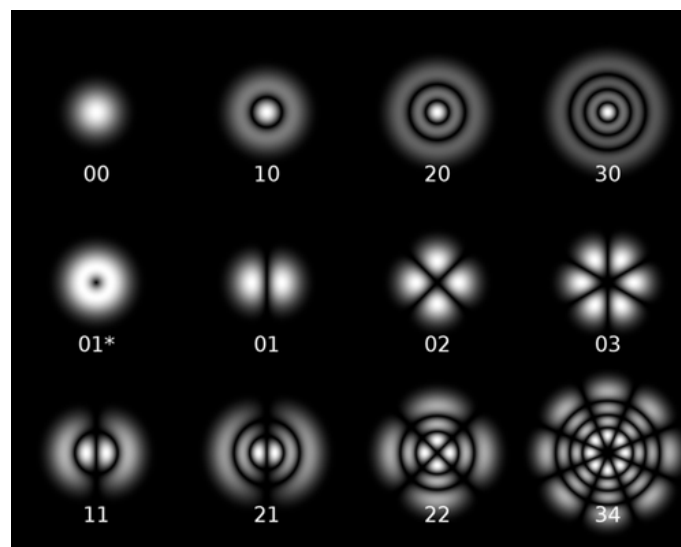

Figure 1.4: Intensity profile of some of the lowest order Laguerre-Gaussian Modes. Note that the phase, not represented in this image, varies across the beam profile. Picture credits:*https* : *//en.wikipedia.org/wiki/Transverse mode*

Note how for both families the mode 00 is the gaussian one.
These modes don't all resonate at the same frequency, but each one has its own

resonance frequency because of the Gouy phase shift: along its propagation direction a beam of a certain shape acquires a phase shift which differs from that for a plane wave; this difference is called the Gouy phase shift. For a gaussian beam the Gouy phase shift is [5]:

$$\phi_G(z) = -arctg\frac{z}{z_R} \tag{1.2.0.2}$$

For the others modes, the Gouy phase shift is different. It's important to note that the mirrors that make up the cavity usually do not have one hundred percent reflectivity, because at least the input mirror must allow the entry of a bit of light. We can calculate the power transmitted to the outside when the system is perfectly in resonance:
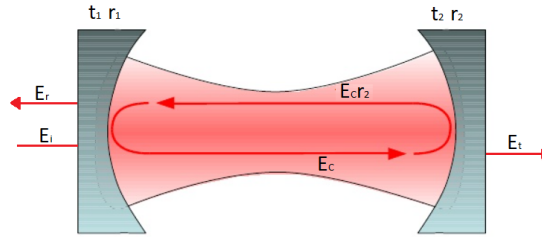

Figure 1.5: Electric fields in a Fabry-Pérot resonator. E_i is the incoming laser field. Inside the cavity the circulating field is given by: $E_c = r_1 r_2 E_c e^{i\phi} + t_1 E_i$. The transmitted field from the mirror 2 is: $E_t = t_2 E_c$, and the reflected field is: $E_r = r_2 t_1 E_c - r_1 E_i$

Called T the percentage of the beam intensity transmitted by a mirror, and R the percentage of the beam intensity reflected by the same mirror, we can define $t = \sqrt{T}$ the transmissivity and $r = \sqrt{R}$ the reflectivity. Now imagining that we have a linear cavity (figure 1.5); the electric field circulating inside the cavity E_c has the following form:

$$E_c = r_1 r_2 E_c e^{i\phi} + t_1 E_i \longrightarrow E_c = \frac{t_1}{1 - r_1 r_2 e^{i\phi}} E_i \tag{1.2.0.3}$$

where E_i is the incident electric field and ϕ is the phase acquired after a complete round trip of the light inside the cavity. $t_{1,2}$ and $r_{1,2}$ are the transmissivity and reflectivity coefficients of the input and output mirrors. The reflected electric field

E_r will be the sum of the promptly reflected input beam and of the beam leaking out from the cavity through the input mirror:

$$E_r = E_c r_2 t_1 - E_i r_1 \qquad (1.2.0.4)$$

From which we can write the reflection factor $Q = \frac{E_r}{E_i}$:

$$Q = \frac{r_2 e^{i\phi} \left[r_1^2 + t_1^2 \right] - r_1}{1 - r_1 r_2 e^{i\phi}} \qquad (1.2.0.5)$$

The intensity of the reflected beam will be:

$$I \propto \mid Q(\nu)E_i \mid^2 \qquad (1.2.0.6)$$

From the equation 1.2.0.3 it is possible to see that E_c reaches its maximum value when ϕ is an integer multiple of 2π.
The free spectral range (FSR), also called axial mode spacing, is the frequency spacing between two adjacent resonances, where E_c reaches its maximum. It is defined as follows:

$$\Delta\nu = \frac{c}{2L} \qquad (1.2.0.7)$$

Another important features that characterize an optical cavity is the finesse (figure 1.6). It is given by the ratio between the free spectral range and the FWHM of the resonance peak:

$$F = \frac{\nu_{FSR}}{\Delta\nu} \qquad (1.2.0.8)$$

it is a parameter that give us an idea of how much a resonator is selective for the resonance frequency. Another way to express the finesse is this:

$$F = \frac{2\pi}{1 - \rho} \qquad (1.2.0.9)$$

where $1 - \rho$ is the fraction of power lost by the beam after one trip inside the cavity.
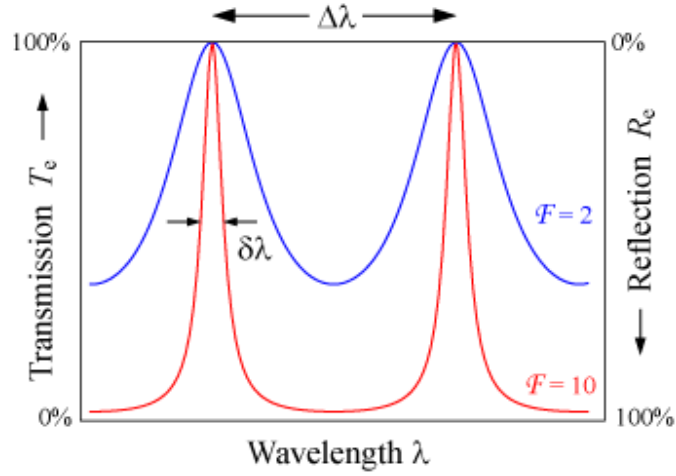
Figure 1.6: Transmitted and reflected power in function of the wavelength. The blue line belongs to a cavity with $F = 2$, the red line belongs to a cavity with $F = 10$. Picture credits: $https://www.rp-photonics.com/finesse.html$

Finally it is possible to define a g_i parameter for each mirrors of the cavity:

$$g_i = 1 - \frac{L}{R_i} \tag{1.2.0.10}$$

where L is the length of the cavity and R_i is the radius of curvature of the mirror $i = (1, 2)$. Using these parameters is possible to calculate the mode that resonates in the cavity. The distances between the two mirrors and the beam waist are given by:

$$z_1 = \frac{g_2(1 - g_1)}{g_1 + g_2 - 2g_1g_2} L \tag{1.2.0.11}$$

and

$$z_2 = \frac{g_1(1 - g_2)}{g_1 + g_2 - 2g_1g_2} L \tag{1.2.0.12}$$

The Rayleigh range follows this formula:

$$z_R = \frac{g_1 g_2(1 - g_1 g_2)}{(g_1 + g_2 - 2g_1g_2)^2} L^2 \tag{1.2.0.13}$$

and the beam waist size is::

$$\omega_0^2 = \frac{L\lambda}{\pi} \sqrt{\frac{g_1 g_2(1 - g_1 g_2)}{(g_1 + g_2 - 2g_1g_2)^2}} \tag{1.2.0.14}$$

Finally the size of the laser beam at the position z_i can be calculated using:

$$\omega_i^2 = \frac{L\lambda}{\pi}\sqrt{\frac{g_i}{g_i(1 - g_ig_j)}} \tag{1.2.0.15}$$

It is therefore possible to make predictions about stability realizing that from 1.2.0.15 and 1.2.0.13, we must to have $0 \leq g_1g_2 \leq 1$ to obtain a real, physically acceptable value for w_0.

1.2.1   Mode Matching

The spatial distribution of the electromagnetic field inside a resonator depends on the shape of the resonator. A given cavity generally supports modes having a well define spatial structure. For example, a parabolic mirrors resonator in homogeneous medium matches a specific gaussian beam, and all the higher orders mode associated with it; what decides which mode resonates, in this condition, is the frequency of the mode. If the frequency of the laser correspond to one of the resonant frequencies of one of these modes, it will resonate, and its intensity will be proportional to how much of that mode was present in the initial beam. The procedure by which you change the shape of the beam so that it couples completely to the fundamental (longitudinal) spatial mode defined by the cavity is called mode matching. To do this type of operation it is possible to use different optical elements, usually lenses or curved mirrors, which allow us change the position and size of the waist.

There is an important relationship for the gaussian beam that links $R(z)$ and $w(z)$ to the so-called complex parameter q:

$$\frac{1}{q(z)} = \frac{1}{R(z)} - i\frac{\lambda}{\pi\omega^2(z)} \tag{1.2.1.1}$$

To describe the change in the beam in going through an optical element, one can use the ray-matrix formalism [2]. The change in the parameter q is computed as:

$$\begin{pmatrix} q_2 \\ 1 \end{pmatrix} = k \begin{bmatrix} A & B \\ C & D \end{bmatrix} \begin{pmatrix} q_1 \\ 1 \end{pmatrix} \tag{1.2.1.2}$$

Where k is a normalization factor and the elements of the matrix depend on the optical component considered. For a mirror with focus $f = R/2$ or a thin lens with focus f the matrix is:

$$\begin{bmatrix} 1 & 0 \\ -1/f & 1 \end{bmatrix} \tag{1.2.1.3}$$

and one obtains:

$$\frac{1}{q_2} = \frac{1}{q_1} - \frac{1}{f} \tag{1.2.1.4}$$

As expected only the real part of $1/q$, the part containing the radius of curvature, is affected by this transformation ; the beam size immediately before and after the mirror or thin lens is unchanged.

1.2.2   Pound Drever Hall Technique

A real optical cavity is not immobile, it is subject to a set of vibrational motions, caused by thermal oscillations, collective movements or external disturbances. Cause the variation of the distance between the mirrors and the consequent variation of the positions of the resonance peaks in figure 1.6. On the other hand, lasers are subject to variation in the emitted frequency which are typically much bigger than the linewidth of a common optical cavity. The Pound Drever Hall technique allows us to obtain an error signal, which can then be used to construct a feedback loop that allows us to maintain the cavity-laser system on resonance, by either actively changing the frequency of the laser to follow the length variations of the cavity, or by actively controlling the length of the cavity to follow the laser frequency fluctuations. An error signal has to give us an information on the offset between laser frequency and resonant frequency of the cavity. If we move from the frequency of resonance to an higher or lower one, we will obtain an increase in the reflected power; this fact, however, does not provide us with any information about our position relative to the resonance frequency, and it is therefore ineffective to build a feedback mechanism. We rather need a system that gives us information about our actual position with respect the resonance frequency. The Pound-Drever-Hall technique (PDH) is used to produce a suitable error signal. The laser is fed into an electro-optic modulator (EOM), which exploits the Pockels effect to introduce an oscillating phase shift, $Asin(\omega_f t)$, to the laser beam. A typical implementation of the PDH technique is shown in figure 1.7:
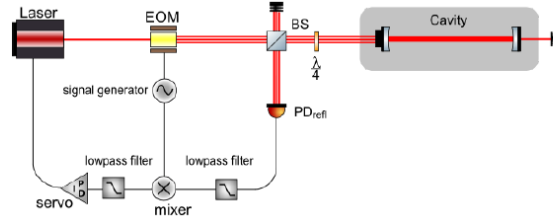
Figure 1.7: PDH servo loop to lock the frequency of a laser to the resonance frequency of a cavity. The laser beam encounters along its path a Faraday isolator and the EOM, which provides a sinusoidal phase modulation. A polarizing beam splitter and a quarter wave plate are used to convey the reflected beam to the photodetector (PD). The signal from the PD is transformed into the error signal that is fed back into the laser's frequency control port.

The laser field, that initially can be represented as $E = E_0 e^{i(\omega t)}$, after passing through EOM, it becomes:

$$E = E_0 e^{i(\omega t + A sin(\omega_f t))} \simeq E_0 e^{i(\omega t)} \left[1 + \frac{A}{2} e^{i\omega_f t} - \frac{A}{2} e^{-i\omega_f t} \right] \tag{1.2.2.1}$$

As we can see, the EOM has introduced two side bands with amplitude $A/2$ and frequency $\omega + \omega_f$ and $\omega - \omega_f$. At this point, the reflected beam will be the sum of these three components, whose field can be written as follows:

$$E_{ref} \simeq E_0 \left[F(\omega) e^{i(\omega t)} + F(\omega + \omega_f) \frac{A}{2} e^{i(\omega + \omega_f)t} - F(\omega - \omega_f) \frac{A}{2} e^{i(\omega - \omega_f)t} \right] \tag{1.2.2.2}$$

Where F is the reflection coefficient of the cavity. When off-resonance, the asymmetric reflection coefficients have the effect of tranforming the phase modulation of the incoming beam into an amplitude modulation of the reflected one. The photodetector reads the power of the reflected laser beam, which is proportional to $| E_{ref} |^2$. This signal is then mixed with the incoming signal from the signal generator (figure 1.7). The resulting error signal has the following form [1]:

$$e = 2\sqrt{P_c P_s} Im[F(\omega)F^*(\omega + \omega_f) - F^*(\omega)F(\omega - \omega_f)] \tag{1.2.2.3}$$

Where P_c is the power of the carrier and P_s is the power of the side bands. The picture 1.8 shows a plot of this error signal.
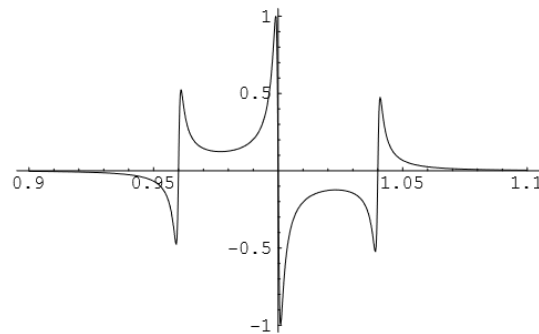
Figure 1.8: Amplitude of the error signal as a function of the frequency of the laser for a cavity with $finesse = 100$, and the modulation frequency that is the 4% of the FSR. In the x-axis there is the frequency in unit of $\Delta\nu_{FSR}$. Credits: Notes on the Pound-Drever-Hall technique, Eric Black.

You can see that through this error signal it is possible to understand what our position is in relation to the resonance frequency, as the sign of the signal changes depending on whether the frequency is above or below the resonance.

1.3   ALPS Experiment

The ALPS (Any Light Particle Search) experiment has the purpose of detecting and study the very light particles at the lower end of the energy scale, the so-called WISP (very Weakly Interacting Sub-eV Particles). The most famous WISP candidate is the axion, introduced to explain the smallness of CP violation in QCD; moreover, the axion is a good candidate to be a constituent of the dark matter.
The experimental setup of ALPS is summarized in a schematic way in figure 1.9.
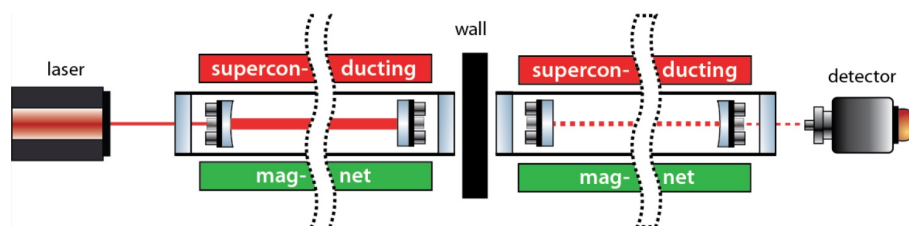

Figure 1.9: Schematic view of the ALPS optical design: the laser beam is fed into a production cavity (the left one);on resonance, the power inside the cavity is about 5000 times higher than the input power. Behind the wall there is the regeneration cavity and the photodetector. The production cavity and the regeneration cavity are both immersed in a magnetic field. Picture credits: Desy, ALPS website, https://alps.desy.de/

The production cavity has the task of generating axions by interaction of the circulating light with a strong magnetic field. The axions do not interact with matter, and are therefore able to cross the wall and reach the regeneration cavity. By interaction of the axion field with the magnetic field, the regeneration cavity has the task of transforming the produced axions into a circulating light, which can be measured by the photodetector.

Given the weakness of the signal (order of 1 photon/week is expected in the regeneration cavity for ideal working condition of the experiments), both the cavities must to be stable and aligned to ensure a good overlap between the optical modes and reduce signal losses due to mode, alignment or frequency mismatch. To make this happen the regeneration cavity length and alignment is controlled using the Pound-Drever-Hall technique and other control system (figure 1.10).
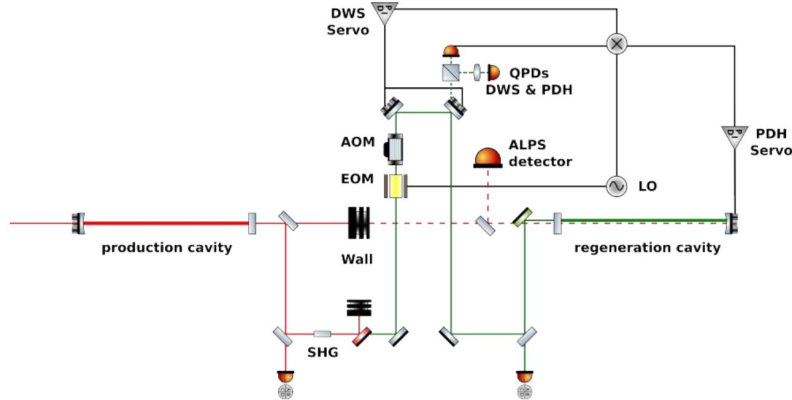

Figure 1.10: Schematic view of the ALPS regeneration cavity including control loop. Picture credits: Desy, ALPS website, https://alps.desy.de/

It is however equally important that the central bench between the two cavities is stable, because any beam shift, introduced by optical components between two cavities, is not seen by the axions traversing the wall and the reproduced light would not match the reference cavity mode. The required length stability for the central bench must be such that the maximum fluctuation do not exceed $100nm$ RMS, and this must to be stable for the duration of the entire experiment, whose minimum time required is a few weeks.

1.3.1   Breadboard

The most common technique to build ultra-stable breadboards is to build monolithic structures by bonding components to a breadboard made of a low-thermal-expansion glass or ceramic [6]. However, the alps experiment requires a light-tight breadboard

to prevent the direct leakage of photons from one optical cavity to the other. This is a problem, since the commonly used low expansion materials (LEM) are not opaque to light. To solve this problem, a composite breadboard was designed by the University of Florida's team.

The materials involved in the construction of the breadboard are aluminum, used for the construction of an opaque coating plate, and ULE (ultra low expansion glass), a titania-silicate low expansion glass with a very low coefficient of thermal expansion; one of the most used materials in this type of applications. The table 1.11 shows the coefficient of thermal expansion, at low and high grades of quality, for the ULE glass. In figure 1.12 is shows the value as a function of temperature of the thermal expansion coefficient for the ULE glass.

LEM	ULE
High Grade	0.0±0.03 ppm/K
Low Grade	0.0±0.1 ppm/K

Figure 1.11: ULE thermal expansion coefficient for lowest and highest grades of quality commercially available. The temperature range is $5 - 35°C$.
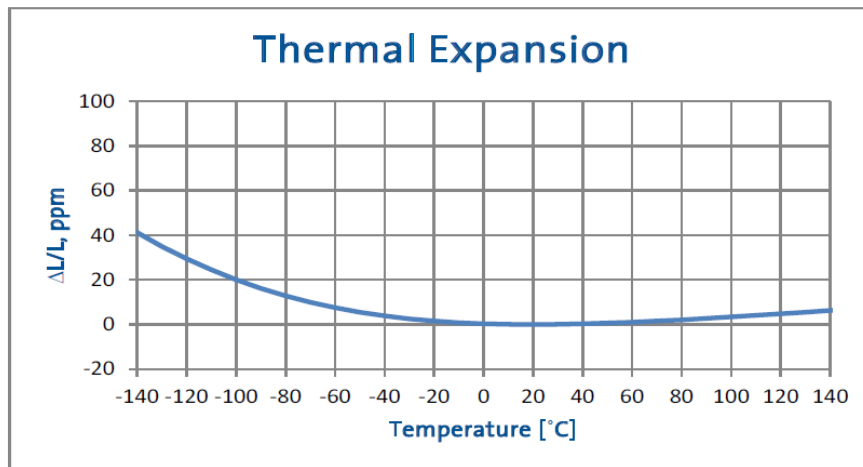
Figure 1.12: Thermal expansion graph for the ULE glass according to the temperature. Credits: Corning ULE 7973 Low Expansion Glass data sheet.

Fig. 1.13 show the breadboard prototype designed at the University of Florida. It consists of a base layer of ULE in which the aluminum optical mounts are anchored; an aluminum panel is placed on the upper part of the base and locked by four screws, this layer serves to make the breadboard light tight. Between the optical mounts and the ULE there is an expansion gap; this is necessary to ensure that the top layer does not affect the stability of the breadboard. The green O-rings in figure 1.13 were then added to ensure that the entire system was opaque to light.
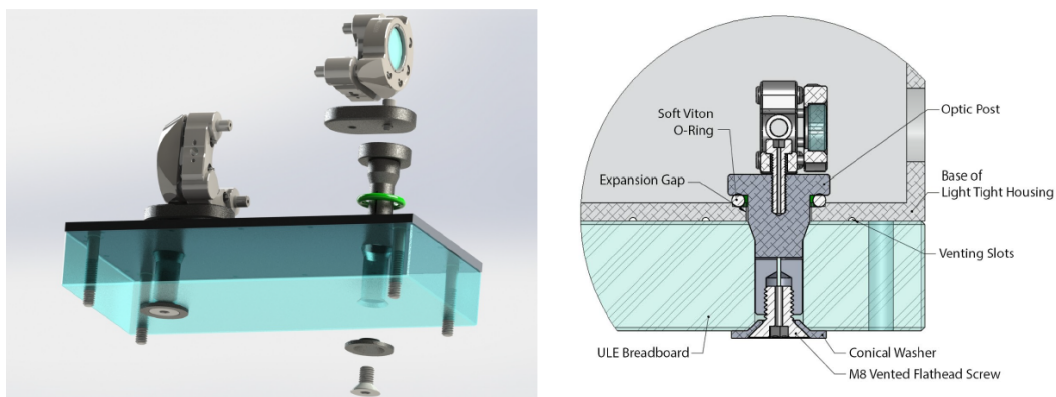

Figure 1.13: Composite light tight breadboard. On the left: a 3D model of the breadboard. On the right: a cross-section of the object. Picture credit: Joe Gleason, University of Florida

The optical mounts are off-the-shelf commercial models (THORLABS POLARIS-K1T3) designed for high thermal stability. Figure 1.14 shows an image of the breadboard used in this thesis work.
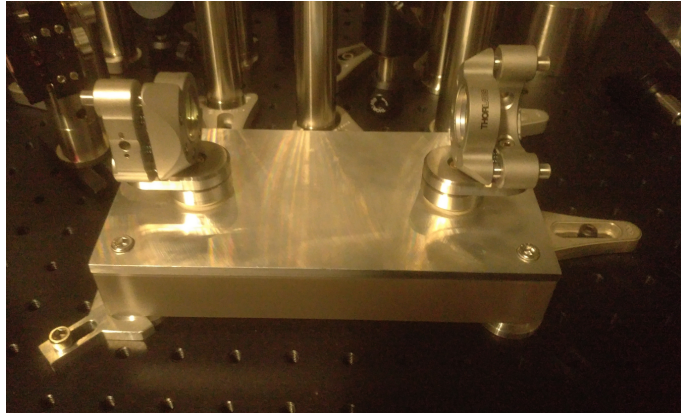

Figure 1.14: Test breadboard used for the longitudinal stability measurement.

Chapter 2

Experimental Setup

In this thesis work, a measurement system has been implemented to verify that the proposed composite breadboard for the central bench of the ALPS experiment meets the minimum stability requirements requested.

The measurement technique here described can be applied to many others precise optical experiments. In the Laser Interferometer Space Array (LISA) project, for example, this measurement technique will be used to control the stability of the spacecraft telescope, but can be also applicable for ground testing of others LISA optical components.

2.1   Experimental Concept

The idea behind this measurement is as follows: two collinear mirrors are mounted in the breadboard to form an optical resonator (which will refer to as "test cavity"); a laser beam (called Laser 2) is mode matched to this cavity and locked to it using the PDH technique (see sec. 2.2.2); the whole system is placed in a vacuum chamber. The same thing is done for an ultra-stable cavity (see sec. 2.3.1), used as a reference cavity, using another vacuum chamber and another laser (called Laser 1). The two lasers locked at resonance to the corresponding cavities, are then made to interfere on a single photodetector, and the frequency stability of the resulting beat note is measured in order to determine the relative length stability of the cavities. Under the assumption that the reference cavity is much more stable than the test cavity (see sec 2.5.1), this is a measurement of the absolute length stability of the test cavity.

Ignoring the Guoy phase term discussed in the paragraph 1.2, which is irrelevant for the purpose of this calculation, the resonant condition in a cavity is reached when an integer number of wavelength fit the round-trip length:

$$\lambda n = 2L \rightarrow \frac{cn}{2\nu} = L \tag{2.1.0.1}$$

Where n is a positive integer and ν is the resonance frequency. Differentiating equation 2.1.0.1:

$$-\frac{cn}{2\nu^2}d\nu = dL \rightarrow -\frac{d\nu}{\nu} = \frac{dL}{L} \tag{2.1.0.2}$$

which gives us the relationship between the variation of the resonance frequency and the variation of the length of the cavity. If the distance between the two mirrors changes, we will see a variation of the relative frequency of the two lasers, i.e. the frequency of the beat note. From equation 2.1.0.2 it is possible to obtain:

$$\frac{dL}{d\nu} = -\frac{L_0}{\nu_0} \tag{2.1.0.3}$$

It is therefore easy to trace the length vibrations once known the variation of the frequency.

2.2   Test Cavity Optical Layout

Fig. 2.6 shows the in vacuum setup for the locking of the beam to the test cavity. The laser beam, before reaching the vacuum chamber of the test cavity, goes through a Faraday isolators, which prevents back-reflected light from the experiment to reach the laser; then a half wave plate and polarizing beamsplitter are used to control the power of the beam without having to act directly on the laser. After this, the laser is fed through an EOM (electro-optic phase modulator) and then reaches the fiber. The prototype breadboard with the test cavity has been set on an optical breadboard using pins, positioned along the perimeter, in order to avoid the stressing of the prototype breadboard from the thermal expansion of the optical breadboard. The system is hosted inside the vacuum chamber equipped with a suspension system capable of attenuating the vibrations from the outside. The laser beam reaches the tank via a polarization-maintaining optical fiber (fiber 2) , which has been suitably coupled with the incoming laser so as to carry a sufficient fraction of power; finally, inside the tank, it reaches the test cavity through a series of mirrors and lenses. This part of the set up, shown in the figure (2.1), consists of a series of seven mirrors and two lenses, through which it is possible to control the mode and the alignment of the gaussian beam to match those of the cavity.
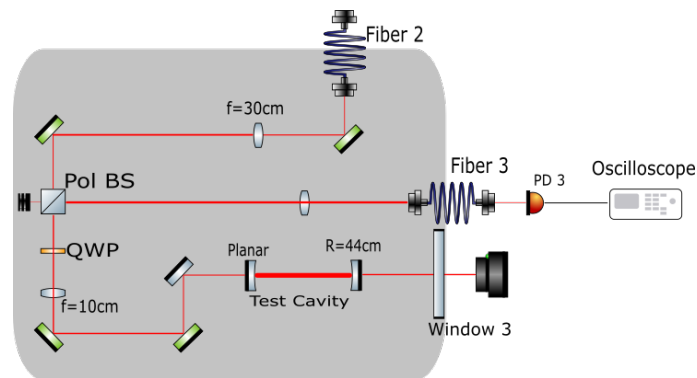
Figure 2.1: In-vacuum part of the optical setup. The laser is injected in the vacuum tanks from fiber 2, coupled to the test cavity (visible in the bottom right) through a series of mirrors and lenses, then it is extracted through fiber 3. The error signal for the cavity locking is detected in-air. A camera in transmission of the cavity helps identify the resonant modes.

A polarized beam splitter (Pol BS) and a quarter wave plate (QWP) were pleced along the optical path; they have the task of conveying the reflected beam from the cavity into the fiber 3; figure 2.2 shows a schematic of the principle of operation.
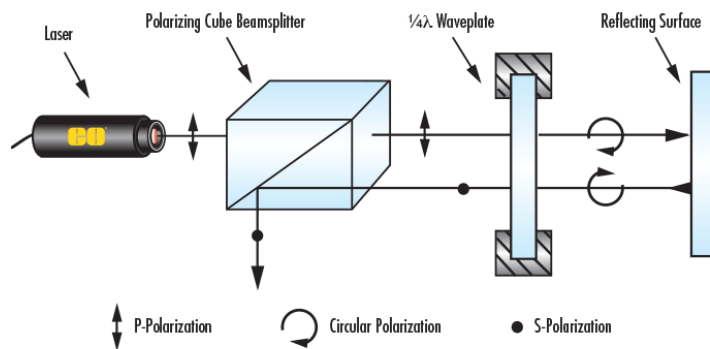

Figure 2.2: The incoming laser beam from the Pol. BS passes through the $\lambda/4$ is reflected by the mirror and comes back, passing again the $\lambda/4$. This changes its polarization by 90 degrees. When the laser beam gets back to Pol BS is diverted in the other direction. Picture credits: *https* : *//www.edmundoptics.com/resources/application − notes/optics/understanding − waveplates/*

The output signal from the fiber is read by a photodetector in-air. In the image 2.3 it is possible to see a photo of the setup, in which the red line shows the path

of the incident laser which comes from the first fiber and the green one shows the reflected beam.
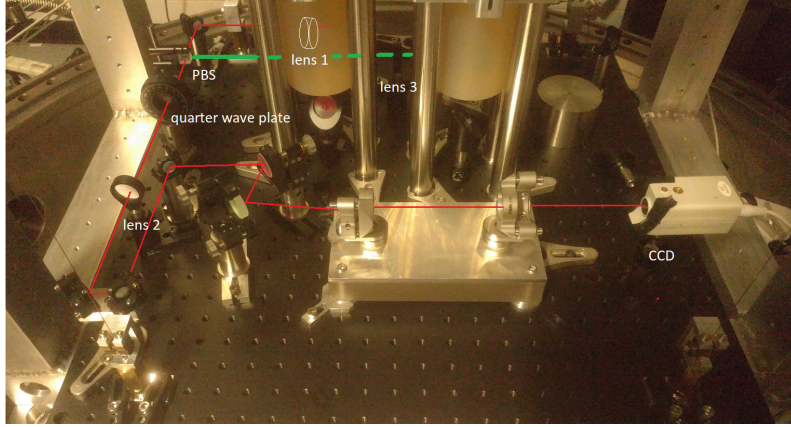

Figure 2.3: Photo of the interior of the vacuum chamber.

2.2.1   Mode Matching of the Test Cavity

We can summarize the basic technical characteristics of the mirrors used for the test cavity in the following table:

Mirrors	Reflectivity	Radius of curvature	Focal Length
Entrance Mirror	~0.993	inf.	inf.
Exit Mirror	~0.995	44.0 cm	22.0cm

Figure 2.4: Mirrors parameters

We list below the characteristics of the obtained cavity knowing that the mirrors are at a distance of 12.0 centimeters, measured with the caliper.
The corresponding free spectral range (FSR) is:

$$FSR = \frac{c}{2L} = 1.25 GHz \tag{2.2.1.1}$$

Assuming that there are no other power losses, the power lost by the light through the mirrors after one trip inside the cavity $(1 - \rho)$, is equal to $1 - R_1 R_2$, resulting in a finesse:

$$F = \frac{2\pi}{1 - \rho} \approx 570 \qquad (2.2.1.2)$$

The geometry of the test cavity implies a precise shape of the gaussian beam that resonate inside it. For a hemispherical cavity, such as the one used in this experiment, the fundamental mode of resonance will be a gaussian mode; it will have the waist located in the same position of the flat mirror, and, at a distance L from the waist, the radius of curvature of the beam will be the same as the curved mirror. Using the formula:

$$R(z) = z\left(1 + \left(\frac{z_R}{z}\right)^2\right) \qquad (2.2.1.3)$$

z_r is uniquely determined and has a value of $10.23cm$, with a beam width at the flat mirror: $\omega_1 = \omega_0 = 0.186mm$ and at the curved mirror: $\omega_2 = 0.258mm$. Alternatively it is possible to achieve the same result using the g factors (see sec. 1.2.1).

As already explained in paragraph 1.2.1, using a system of lenses it is possible to modify the position and the width of the input beam waist to match the cavity mode. We used two lenses, one with focal lenght $f_1 = 30cm$ and the other with $f_2 = 10cm$.

Through a procedure called beam-Scan, the position and size of the waist of the beam leaving the fibre 2 have been measured; this operation consists in measuring the transverse intensity profile of the laser beam at several position along the optical axis, computing the beam size and comparing it with eq. 1.1.0.8 to extract the parameters of the gaussian beam. In our case we used a WinCAM, a dedicated tool consisting of a CCD camera and it associated software. The positions of the lenses were chosen using a program called JAMMT, which, starting from the parameters of the initial beam, can calculate the positions of the lenses to obtain the desired Gaussian beam. Lens 2 was at the distance of 56.4cm from the cavity, and the lens 1 was at 97.3cm from the cavity.

To fine tune the alignment, adjusting two mirrors just before the cavity, we tried to minimize the reflected power (figure 2.5) at the TEM_{00}, remembering that the maximum drop is obtainable from the formula 1.2.0.5.
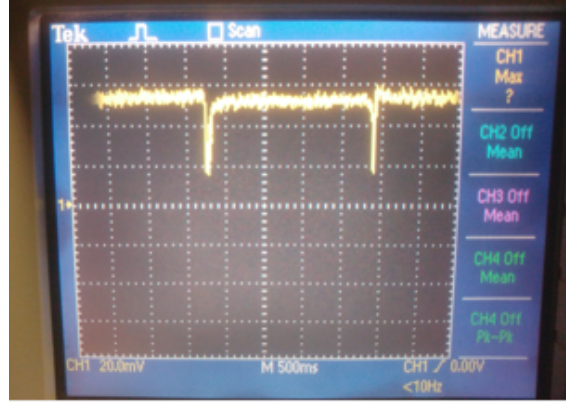
Figure 2.5: Power drop in correspondence of the 00 mode on the oscilloscope, the signal is coming from the photodetector 3.

This operation has been carried out going to modify the inclinations of the two mirrors immediately before the cavity, in order to obtain a perfectly mode match.

2.2.2   Feedback Signal

The signal coming from the photodetector 3 (figure 2.6) is sent to the mixer in order to create the error signal, as shown in figure 1.7. The signal thus formed is digitized and read by a computer, which, through a custom program written in LabView, controls the digital PID (Proportional-Integral-Derivative) filter, that adjusts the output according to the value of the error signal (proportional), the past values of the error signal (integral) and how fast the error signal varies (derivative). This filter has the task of transforming the PDH error signal into an output used to control the feed-back on the laser frequency and keep it locked on resonance.
With the aim of optimizing the error signal, it is possible to appropriately select the amplitude of the phase modulation on the EOM, so that the slope of the error signal is maximum. Another parameter that needs to be optimized to get a stable lock is the gain; called e(t) the error signal, the control signal u(t) sent from the PID to the laser piezo has this form:

$$u(t) = K_p e(t) + K_i \int_0^t e(\tau)\, d\tau + K_d \frac{de(t)}{dt} \qquad (2.2.2.1)$$

where K_p is the proportional gain, K_i is the integral gain and K_d is the derivative gain.

2.3   Final Setup

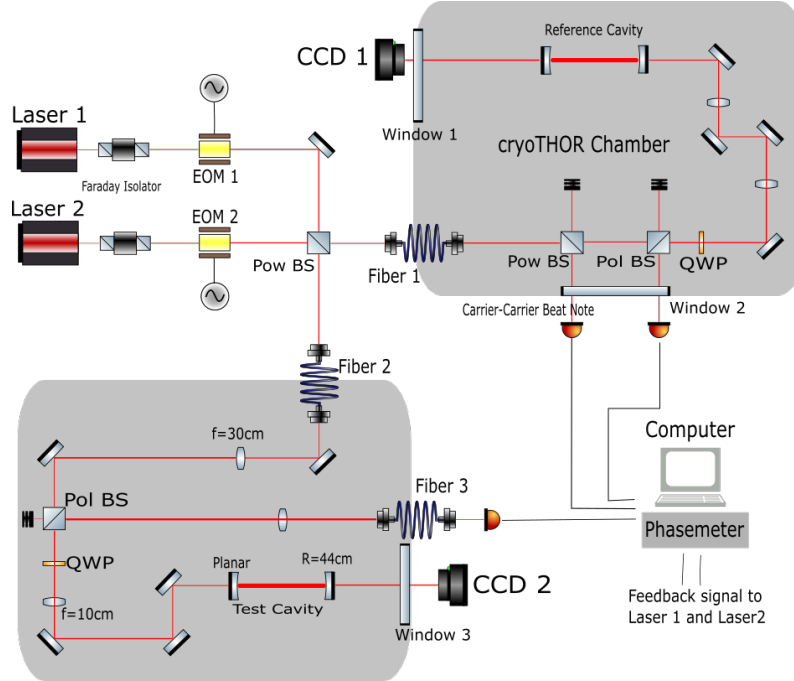A simplified diagram of the experimental setup is shown below (figure 2.6).

Figure 2.6: Complete path of the experiment with both cavities.

The total system consists of two vacuum chamber: the CryoTHOR one (an existing experimenter for which the test cavity was previously used), and the test tank. The Laser 1 and the Laser 2 are both controlled through a computer, which allowed us to act on the piezo of the lasers. The beams generated by them pass in succession a Faraday isolators, a half wave plate, and a polarizing beamsplitter. They reach the respective EOM, which both provide amplitude modulation with $A = 0.105V$ but at different frequencies. Before reaching the fibers for the vacuum chambers, the laser beams coming from both the laser 1 and the laser 2 are recombined at a power beam splitter as shown in figure 2.6. This is essential for the generation of the carrier-carrier beat note. In the same figure is possible to note the path for the reference cavity, already present in the CryoTHOR experiment.

2.3.1   Reference Cavity

As already explained, we need a reference cavity to provide a reference frequency with which to compare the frequency of the laser locked to the test cavity. The

superposition of this two signals generates an oscillating amplitude signal (carrier-carrier beat note), that can be read by the data acquisition system.

The reference cavity is composed of a monolithic space in zerodur, at the ends of which two fused silica mirrors are attached. The zerodur is a lithium aluminosilicate glass-ceramic, used widely in the construction of mirrors for very large telescope because of its mechanical and physical properties. The table 2.7 shows the zerodur thermal expansion coefficient.

LEM	Zerodur
High Grade	0.0±0.02 ppm/K
Low Grade	0.0±0.1 ppm/K

Figure 2.7: Zerodur thermal expansion coefficient for lowest and highest grades of quality commercially available. The temperature range is $5 - 35°C$.

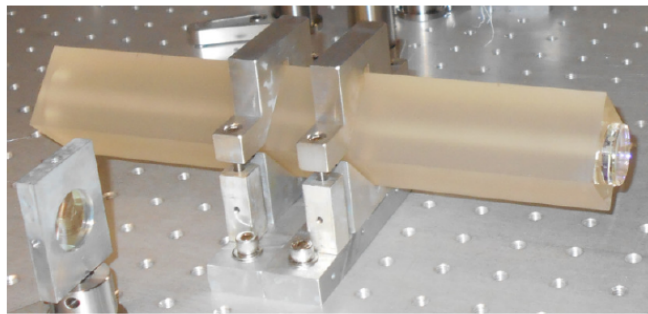The reference cavity is 23.1cm long. A picture of it is shown in 2.8.

Figure 2.8: Zerodur reference cavity used already for the CryoTHOR experiment.

The basic parameters are shown in the table 2.9.

Length	23.1cm
R₁	50cm
R₂	100cm
Finesse	21 000

Figure 2.9: Table with the properties of the reference cavity.

The stability of the reference cavity has been already studied by Johannes Eich-holz during his thesis work. The reference system performance is shown in figure 2.10
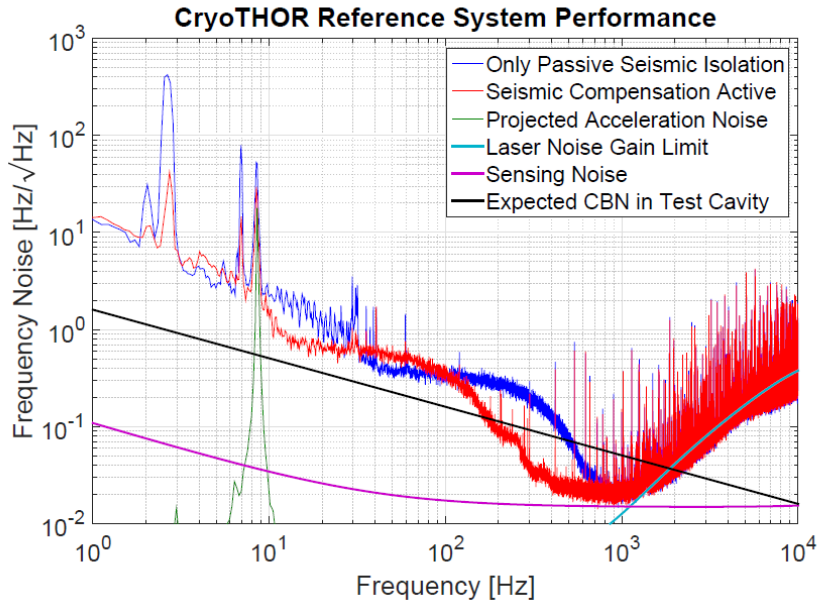

Figure 2.10: CryoTHOR reference system performance. The sensing limit represents the combined phase noise due to shot noise, PD technical noise, and ADC quantization noise. The gain limit represent the laser feedback's inability to suppress the differential noise between laser and cavity due to insufficient bandwidth [3]. The frequency noise is expressed in $Hz/\sqrt{Hz}$; to pass from it to $m/\sqrt{Hz}$ it is sufficient to use the equation 2.1.0.3, the conversion factor is $4.26 * 10^{-16}$

Length	23.1cm
R_1	50cm
R_2	100cm
Finesse	21 000

2.3.2   Phasemeter

The main function of the phasemeter is to provide an accurate measurement of the phase or frequency of an input signal. To do this it exploits a digital phase-locked loop (DPLL) to track the phase of the signal.
The output signal from the photodetector can be represented as follows:

$$X(t) = A_x sin(\omega t - \Phi_x(t)) \tag{2.3.2.1}$$

With ω a constant. We are interested in the behavior of the phase, because it contains the information on the fluctuations of the cavity. Figure 2.11 shows a schematic of the DPLL circuit:
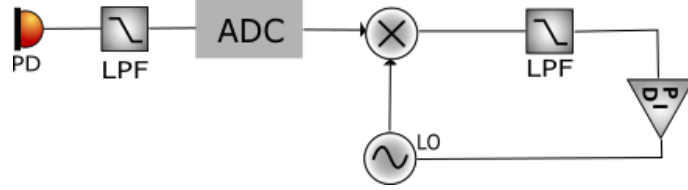

Figure 2.11: The input signal, once digitized (ADC), is mixed with the signal coming from a local oscillator (LO) and injected into a low pass filter. The signal formed acts as an error signal for the updating of the phase of the local oscillator.

We can consider the signal from the LO as:

$$Y(t) = A_y sin(\omega t - \Phi_y(t)) \tag{2.3.2.2}$$

By multiplying the two signals on the mixer, and applying the filter, it is possible to generate an error signal Q(t):

$$Q(t) = \frac{kA_yA_x}{2}sin(\Delta\Phi(t)) \tag{2.3.2.3}$$

Where k depends on the gain of the mixer. The system drives this signal to 0 so that there is no phase difference between the input signal and the signal from the local oscillator. The updating of the LO phase is not instantaneous. To track and correct for the error due to the update delay, important especially at high frequency, it is necessary the implementation of the IQ readout scheme represented in figure 2.12.
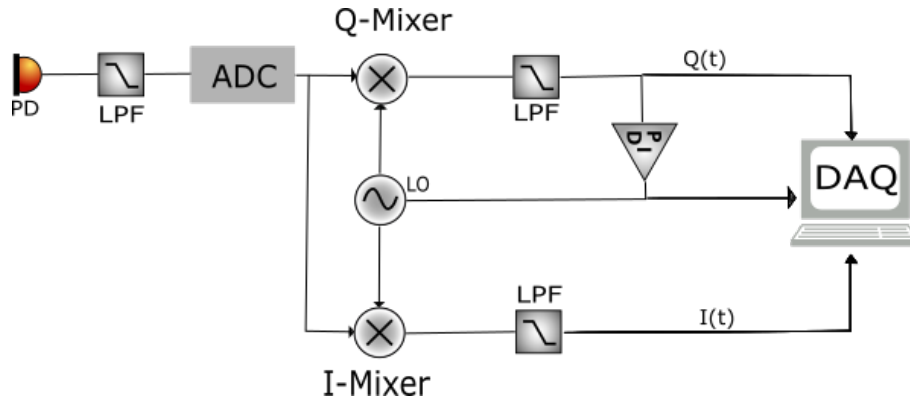
Figure 2.12: The input signal is also multiplied with a second mixer and fed into a low pass filter. The signal formed is called I(t)

The signal I(t) can be written in the following form:

$$I(t) = \frac{kA_y A_x}{2} cos(\Delta\Phi(t)) \tag{2.3.2.4}$$

You can then estimate the phase $\Delta\Phi(t)$ as:

$$\Delta\Phi(t) = arctg\left(\frac{Q(t)}{I(t)}\right) \tag{2.3.2.5}$$

This information can be used to correct the estimated phase of the local oscillator.

2.3.3   Generation of the Beat Note

Once the system is complete, it is possible to proceed to lock each laser to its respective cavity. The resonances of the two cavities to which to lock have been chosen in such a way that the frequency difference between the two lasers was less than 32MHz. This choice is due to the fact that the sampling frequency of the phasemeter is 64MHz; to avoid aliasing problems, the sampling rate must be at least double to that of the input. The beat note contains information on the difference in frequency between the two carries, indeed, the signal read by the photodetector is:

$$I = [A_1 e^{(\omega_1 t)} + A_2 e^{(\omega_2 t)}]^2 \tag{2.3.3.1}$$

From which:

$$I = P_1 + P_2 + A_1 A_2 [cos((\omega_1 - \omega_2)t)] \tag{2.3.3.2}$$

The amplitude of the resulting signal oscillates at a frequency f equal to $\nu_1 - \nu_2$. Since ν_1 is the resonance frequency of the reference cavity, it is possible to consider it constant, and write the phase of the beat note as follow:

$$\Phi(t) = 2\pi(\nu_1 - \nu_2(L))t \qquad (2.3.3.3)$$

Where $\nu_2(L)$ is the resonance frequency in function of the length of the test cavity (equation 2.2.0.1).
This signal coming from the photodetector is fed into the phasemeter, which tracks the frequency of the incoming signal and return us the relative phase between the input and an internal reference. However, we are interested in variation of this frequency, and not to the absolute value of the frequency; indeed the information of the stability of the cavity is contained in the relative shift between the resonance frequencies of the test cavity and the reference cavity, in other words, the resonance frequency of the reference cavity is the zero point for the frequency changes.

Chapter 3

Results

To study more accurately the beat notes, the incoming signal to the data acquisition system was split through a T-junction, so it is possible to control the spectrum of the signal through a spectrum analyzer. This device allows us to visualize on the screen the spectral decomposition of the analyzed signal. In our specific case, it allowed us to check that we were choosing two TEM_{00} resonances on the two cavities which were spaced by no more than 32MHz (which is the maximum frequency of the beat signal we can measure with the phasemeter).

Two sets of measurements were made to assess the stability of the test cavity. The first is a rough study of the breadboard's stability dependence on medium/long term temperature fluctuations, carried out by manually collecting data with the aforementioned spectrum analyzer. The second one is a real-time measurement of stability of the breadboard, from which we can obtain a noise spectrum. In this case, the data acquisition is managed by a computer, which controls the phasemeter.

3.1   Temperature Dependence

The material that makes up the base of the breadboard is ULE (Corning ULE 7973 Low Expansion Glass). The technical sheet of the material shows a value for the linear coefficient of thermal expansion of $0 \pm 100 ppb/°C$ from $5°C$ to $35°C$, which is the temperature range of interest for our experiment. For a $12cm$ long pure ULE cavity, one can expect a maximum thermal expansion (or contraction) of about $12nm/°C$. However, since what we are interested to study in this case is not only the breadboard itself, but also the optical mounts and the posts that support them, we expect a somwhat higher value of thermal expansion for the whole cavity.

The measurement of the breadboard temperature dependence has been carried

out by taking advantage of the natural temperature variations in our lab. A digital thermometer was applied to the external wall of the test vacuum chamber to monitor these variations; the thermometer was not applied inside of the tank because of technical issues. The vacuum pumps were not activated, so that the system was in air at atmospheric pressure; nevertheless, the vacuum chamber provided a closed environment protected from air turbulence and small scale temperature fluctuations. Both lasers were locked on resonance of the two cavities and the beat note between the two carriers was measured using the spectrum analyzer; the value was recorded manually over the period of a week.

Table 3.1 shows the collected temperature and frequency data as a function of time:

Time [h]	Frequency Shift [MHz]	Temperature [°C]
0	-52,6	20,8
17	-29,1	20,6
20	-47,9	20,7
40	-29,6	21
63	-97,4	21,1
88	-86,9	21
90	-75,6	21
115	-62,9	29,9
160	-44,1	20,8

Figure 3.1: Temperature of the vacuum chamber and frequency shift of the beat note between the lasers locked to the two cavities as a function of time. The frequency shift is relative to the initial frequency. The frequency measurements are affected by an error $\sigma = 0.1 MHz$ due to the positioning of the cursor. The error for the temperature measurement is $\sigma = 0.05°C$

Since the lasers used are infrared lasers with a wavelength of about $1.064\mu m$, using formula 2.2.0.4 it is possible to estimate the relationship between frequency variation and variation of cavity length. We get that for the test cavity:

$$\frac{dL}{d\nu} \simeq -0.426 nm/MHz \tag{3.1.0.1}$$

Figure 3.2 shows a comparison between temperature fluctuations and the variation of the test cavity length, calculated using 3.1.0.1 and assuming that the variation in length of the reference cavity is much smaller and can be neglected.
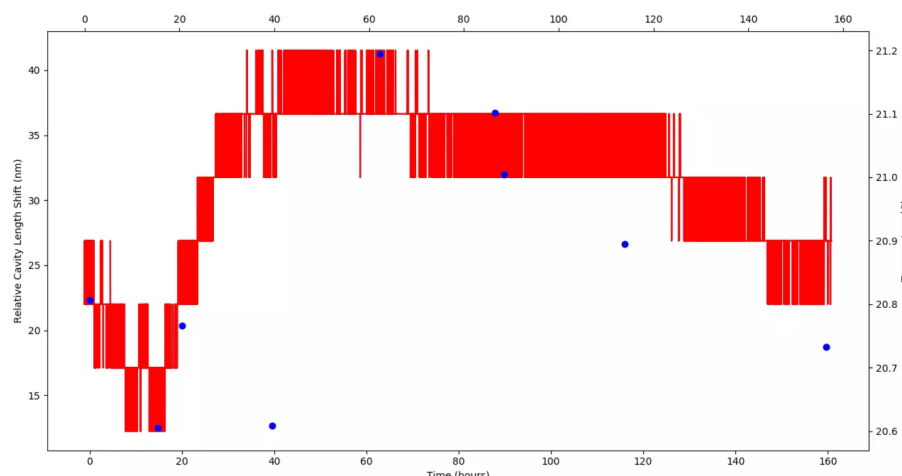
Figure 3.2: Correlation between the temperature (red band) and the relative cavity length shift (blue points).

The graph shows that there is an appreciable correlation between temperature and length variation. We can use the data present in table 3.1 to estimate the coefficient of thermal expansion at ambient temperature of the test cavity, and then compare it with that of ULE at the same temperature.

In the first 40h, the room temperature fluctuated from 20,6 to 21,2°C. Between 50 and 160 hours, the temperature drops slowly, from 21,2 to 20,8 degrees; since the variation is very slow, we can assume that the temperature inside the chamber was fairly uniform and the delay with respect to the external temperature negligible. We can the use the data recorded in this period of time to estimate the thermal expansion of the composite breadboard.

The coefficient obtained is $60 \pm 10 nm/°C$. This result was obtained by calculating the thermal expansion for each set of measurements (row) in table 3.1, and then averaging the results; the temperature change was slow enough to allow us to consider delay between the temperature variations at the wall of the vacuum thank and those at the breadboard.

The obtained thermal coefficient is much larger than what is expected by the expansion of the ULE breadboard alone. This difference is likely due to the composite nature of the breadboard; we may think that the excess susceptibility of the cavity to thermal variation is due to a sum of several factors:

- The aluminum layer placed over the base of ULE could create a stretching stress.

- Movements of the anchoring posts of the optical mounts.

- Holders and mounts thermal expansion.

It must be noted, however, that any length shift due to local deformations of the optics holders or the anchoring posts does not depend on the length of the breadboard, and its impact on the overall length stability will scale inversely with the length of the cavity.

3.2 Frequency Noise

The second set of measurements is a spectral density analysis, using the computer-controlled phasemeter as the data acquisition system. This measurement gives us information about the stability of the structure at different frequencies, so it is one of the most used methods of stability analysis. To minimize low-frequency noises due to thermal drift and air turbulence, the test chamber has been evacuated. The measurement was accomplished by sampling the beat note with a frequency of 30Hz for a total time of one hour. Figure (3.3) shows the power spectral density of the test cavity length fluctuations.
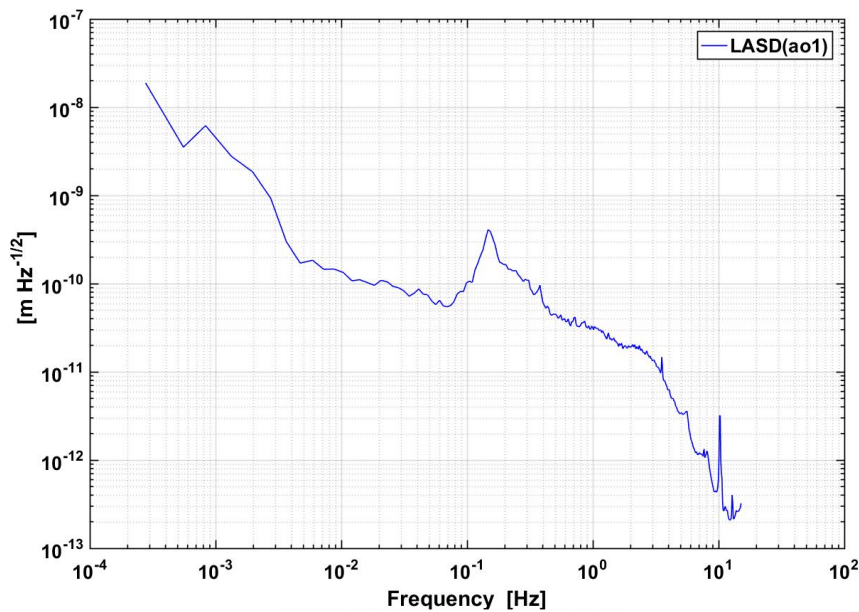

Figure 3.3: Noise amplitude spectral density. We monitored the length of the cavity for 1h using a sampling frequency of 30Hz.

Periodic noise sources are characterized by sharp peaks in the spectrum. With the aim of studying a larger spectrum of frequencies two measures were also

carried out with a much higher sampling rate, 125kHz, for an acquisition time of about twenty seconds (figure 3.4).
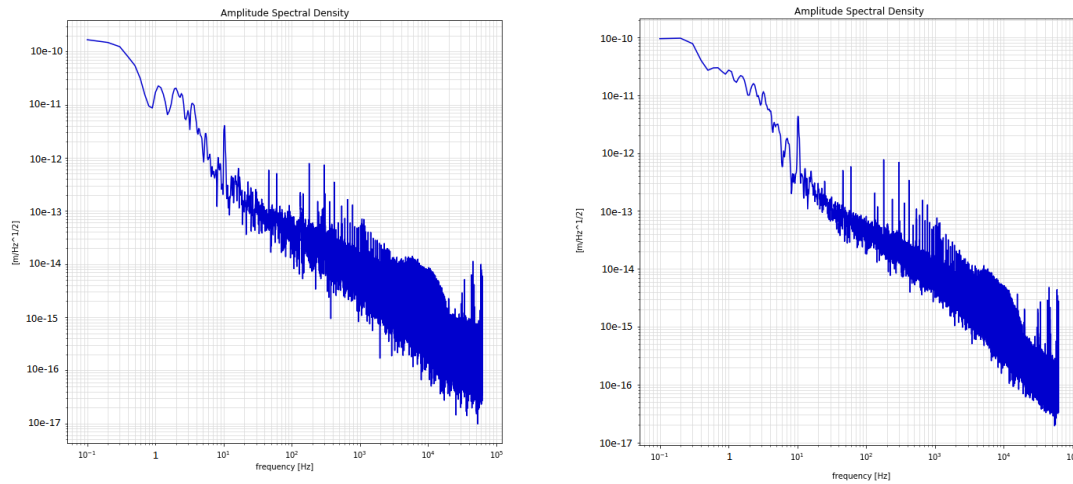

Figure 3.4: Noise amplitude spectral density. We monitored the length of the cavity for about 20s using a sampling frequency of 125kHz.

At 10kHz the amplitude spectral density reaches the level of the reference system noise (figure 2.10). It is therefore possible to consider the breadboard vibration dominant in the amplitude spectral density under the 1kHz.

Chapter 4

Conclusions

4.1 Considerations on Thermal Dependence

The measurement carried out in air have shown an evident dependence of the breadboard on the thermal oscillations. The room temperature has been monitored for about 160 hours. Figure 3.2 shows the temperature oscillation during this time.
The thermal expansion found for the test cavity is $60 \pm 10 nm/^{\circ}C$. As we can see from figure 2.9, the material that makes up the base of the composite breadboard (ULE), at working temperatures, has a coefficient of thermal expansion of $0 \pm 0.1 ppm/^{\circ}C$. This, for a 12cm long cavity, become $0 \pm 12 nm/^{\circ}C$. However, we must remember that we are studying a composite breadboard, and it is necessary to consider also the contribution of the mirror mounts, supporting posts and possibly the stretching stress caused by the aluminum layer.
We can think the coefficient of expansion of our cavity as the sum of three contributions: one from the holders, one from the aluminum layer, and the ULE base contribute.

$$c_{tot} = c_{base} + c_{holders} + c_{layer} \qquad (4.1.0.1)$$

In subsequent estimates we will assume negligible the stress force caused by the aluminum layer, since in the breadboard are present expansion gaps in order to avoid this type of problem.
If we consider that the maximum contribution from the ULE base to the coefficient of thermal expansion is $12 nm/^{\circ}C$, we can assume that the remaining $48 nm/^{\circ}C$ is a lower bound for the thermal expansion provided by the mirror mounts. However, it is important to note that the thermal expansion coefficient of the holders does not depends on the length of the breadboard, but it is a constant value to consider when we are using this type of holders.

4.2   Considerations on Frequency Noise

The spectrum of the 30 Hz measurement has two evident peaks, one at about 0.2Hz and the other at 10Hz. The nature of these peaks is unknown: they can be caused by external noises or by resonances of the system; in the latter case, they may need to be mitigated by stiffening the structure of introducing damping mechanisms. The drift at lower frequencies can be traced back to slow thermal fluctuations, to which the cavity, despite being in vacuum, is still subject.

It is possible to see that above 10Hz the amplitude spectral density is always under $1pm/\sqrt{Hz}$. Between 1 and 10^3 Hz the noise caused by the reference system (see figure 2.10) is different orders of magnitude under the amplitude spectral density measured; we can hypothesize that, in this range, the vibration of the test cavity are dominant. This information on the stability of the prototype breadboard can helps to design properly the central bench for the ALPS experiment.

Bibliography

[1] Eric Black. Notes on the Pound-Drever-Hall technique. Technical note, LIGO, 1998.

[2] Anthony E. Siegman. Lasers. University Science Books, 1986.

[3] Johannes Michael Eichholz. Digital Heterodyne Laser Frequency Stabilization for Space-Based Gravita- tional Wave Detectors and Measuring Coating Brownian Noise at Cryogenic Temperatures. PhD thesis, University of Florida, 2015.

[4] Daniel Shaddock et al. Overview of the LISA Phasemeter. Online; accessed 20-July-2018.

[5] Rüdiger Paschotta. The Encyclopedia of Laser Physics and Technology. Online; accessed 20-July-2018.

[6] S. Lucarelli, D. Scheulen, D. Kemper, R. Sippel, D. Ende, A.Verlaan, H. Hogenhuis. The Breadboard Model of the LISA Telescope Assembly. Online; accessed 9-September-2018.